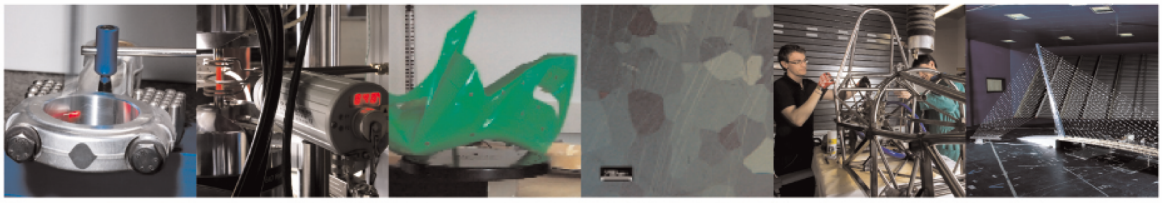

On monitoring fretting fatigue damage in solid railway axles by acoustic emission with unsupervised machine learning and comparison to non-destructive testing techniques

Michele CARBONI, Marta ZAMORANO

This is a post-peer-review, pre-copyedit version of an article published in Proc IMechE Part F: J Rail and Rapid Transit. The final authenticated version is available online at: https://doi.org/10.1177/09544097231193186

DIPARTIMENTO DI MECCANICA ■ POLITECNICO DI MILANO
via G. La Masa, 1 ■ 20156 Milano ■ EMAIL (PEC): pecmecc@cert.polimi.it
http://www.mecc.polimi.it
Rev. 0

On monitoring fretting fatigue damage in solid railway axles by acoustic emission with unsupervised machine learning and comparison to non-destructive testing techniques

Michele CARBONI[1*], Marta ZAMORANO[2]

[1] *Politecnico di Milano, Dept. Mechanical Engineering, Via La Masa 1, 20156 Milano, Italy*
[2] *Universidad Carlos III de Madrid, Dept. Mechanical Engineering, Av. de la Universidad 30, 28911, Leganés, Madrid, Spain*

Abstract

Railway axles are safety-critical components of the rolling stock and the consequences of possible in-service failures can have dramatic effects. Although this element is traditionally designed against such failures, the initiation and propagation of service cracks are still occasionally observed, requiring an effective application of non-destructive testing and structural health monitoring approaches.
This paper investigates the application of structural health monitoring by acoustic emission to the case of solid railway axles subject to fretting fatigue damage. A full-scale test was performed on a specimen in which artificial notches were suitably manufactured in order to cause the initiation and evolution of fretting fatigue damage up to the stage of relevant propagating fatigue cracks. During the test, both periodical phased array ultrasonic inspections and continuous acquisition of acoustic emission data have been carried out. Moreover, at the end of the test, the specimen was inspected, analyzed and evaluated by visual inspection and magnetic particles testing, while acoustic emission raw data were post-processed by a special unsupervised machine learning algorithm based on an Artificial Neural Network. It is demonstrated that the proposed methodology is very effective to detect the onset of crack initiation in a non-invasive and safe way.

Keywords: fretting fatigue, solid railway axle, non-destructive testing, ultrasonic phased array testing, structural health monitoring, acoustic emission, unsupervised machine learning

[*] Corresponding author: Tel.: +39-02-23998253, Fax: +39-02-23998202, e-mail: michele.carboni@polimi.it (M. Carboni).

1 Introduction

A railway axle is a safety-critical component of the rolling stock. Its structural design approach is traditionally based on the fatigue limit, as indicated by relevant standards (EN13261 [1] and EN13260 [2] plus EN13103-1 [3] or EN13103-2 [4] in Europe or AAR Section G [5] in North America). Considering the exemplificative European approach, five different full-scale fatigue limits, to be experimentally estimated by suitable full-scale fatigue tests, are defined, and associated to different regions of an axle: for example, the fatigue limit to be considered for the external body surface is typically different with respect to that for press-fitted surfaces. This because, generally, the acting loading conditions and the damaging phenomena change between different regions of an axle.

Focusing on solid railway axles, this research deals with fretting fatigue damage [6]-[8], a phenomenon causing unexpected premature service failures located at the seats between an axle and the press-fitted wheels, brake discs or gear wheels [9]. Fretting consists of [8] the repetitive micro sliding, due to the applied loads and to vibrations, of two surfaces put in contact in a press-fit connection. In presence of favorable conditions, fretting causes a fatigue surface damage initially characterized by wear, but, then, evolving into multiple-site initiation of shallow surface micro cracks gradually coalescing to form major surface shallow cracks. If the applied cyclic load levels and the depth of such major shallow cracks are high enough, their propagation is driven, by the applied bulk stress, up to the final failure of the axle. Due to fretting fatigue damage, the literature reports decrements of fatigue life in the order of 60%–75% [6], [8], [10].

To mitigate the issue of fretting fatigue in railway axles, different approaches are proposed in the literature. The first introduced one involved a more effective structural design of railway axles against fretting fatigue, also complementing the traditional method based on the fatigue limit by more refined design tools [11]-[18]. Nevertheless, in-service failures of axles, although decreased, were still occasionally observed.

The second approach, the most widespread in the present scenario of European railway applications [19]-[20], starts from the first one and adds, according to a Damage Tolerant [21] approach, in-service periodical non-destructive testing (NDT) [22] inspections by, for example, visual testing (VT), magnetic particle testing (MT) and conventional mono-crystal ultrasonic testing (UT). Such inspections are performed at suitable (and expensive) service interruptions planned for maintenance operations. Nevertheless, in-service failures have not been totally eliminated yet.

The third approach, the newest and the less developed, is focused on implementing tools and methods for real time or on demand structural health monitoring (SHM) of railway axles. SHM has shown, especially in the aeronautical and civil fields [23]-[24], the opportunity, with respect to NDT, to decrease the costs by 30% without losing accuracy.

Few studies are available in the literature on SHM applied to railway axles and none, for what the authors know, specifically on monitoring fretting fatigue damage. Nevertheless, the more mature proposed approaches for axles seem to be acoustic emission [25]-[29], low frequency vibrations (revolution periodicity) [30], high frequency vibrations (shifting of natural frequencies) [31] and automated UT [32].

Among the above-mentioned SHM approaches, this study deals with acoustic emission (AE) [33]-[34] because, today, it seems to be one of the most mature and because the needed equipment is light, small in size and easy to handle (very important considering the application to axles mounted on running trains). Moreover, in the railway field, AE is already successfully applied for monitoring rail-wheel interaction and for detecting faults in axle bearings, welded bogies and tracks.

In the industrial field, AE is a passive SHM technique [34] based on the concepts of seismology applied to a smaller scale and to different types of material. It relies on the fact that, when any damage evolves in a material, it releases energy in terms of ultrasonic elastic waves (“micro-earthquakes”), which can be acquired, post-processed and interpreted to get useful information on the developing damage itself. Such AE “hits” (Figure 1 [29], which describes some of the features typically used to fingerprint the acquired

waveforms, as well) are typically short and transient ("burst events") and have a frequency bandwidth within the 100–1000 kHz range.
A critical point of AE monitoring is the huge amount of data to be managed, which is not just directly related to damage phenomena, but also to the presence of background noise and interferences. This requires applying tools from the field of Big Data Analytics and Data Science [35] due to the need to cluster AE raw data. To the aim, pattern recognition techniques proved to be a suitable tool [36] and, in the literature, the adoption of unsupervised [37] algorithms is suggested [33], for the specific case of AE, because they do not require to know the output a priori, but allow to arrange their architecture according to the input.

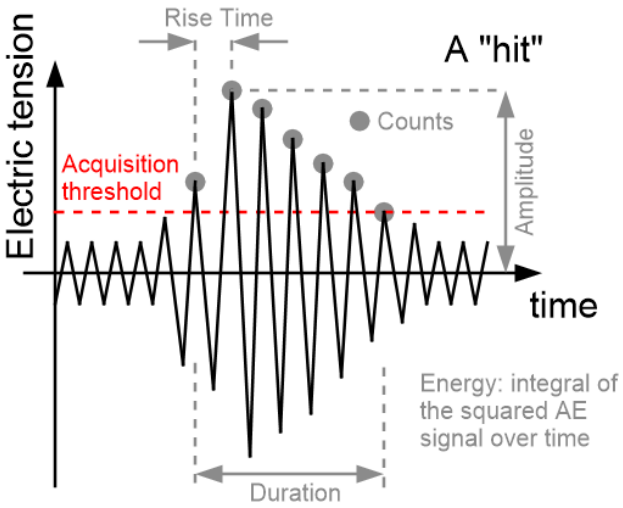

Figure 1. Scheme of an AE hit (case of burst event). [29]

This paper investigates the application of SHM by AE to the case of solid railway axles subject to fretting fatigue damage. A full-scale test was performed using a Vitry test rig, i.e., a three-point rotating bending bench, on a sample in which artificial notches were manufactured to trigger and to make evolve fretting fatigue damage up to the stage of relevant propagating fatigue cracks. During the test, both periodical phased array UT (PAUT) [38] inspections and continuous acquisition of AE data have been carried out. For what the authors know, the application of PAUT to inspect fretting fatigue damage in solid railway axles is a novelty, as well. Moreover, at the end of the test, the surfaces subjected to fretting action were inspected, analyzed and evaluated by VT and MT, while AE raw data were post-processed by a special unsupervised machine learning algorithm based on an Artificial Neural Network (ANN) [39]. The obtained results were compared to and validated by the mentioned NDT inspections.
It is important to mention that the proposed AE monitoring approach has been previously, fully and successfully investigated and validated considering the case of the free external body surface of solid axles [29]. The present research, therefore, is a step forward in the application of the approach to the more difficult case of fretting fatigue damage at press-fit seats.

2 Experimental setup

In this section, the experimental full-scale test is described, as well as the acquisition system used for AE monitoring. The here-considered full-scale test was originally part of a wider research program focused on

the mechanical characterization and modelling of fretting fatigue damage in railway axles. All the details and results about this research program can be found in [12]-[13] and [16].

2.1 Description of the full-scale test

A full-scale specimen was tested according to the suggestions provided by EN 13261 [1] for press-fitted assemblies. The specimen was made of EA4T steel grade (quenched and tempered 25CrMo4 steel) and a scheme of its solid geometry is shown in Figure 2a. A diameter ratio D/d equal to 1.12 (D = 165 mm and d = 147 mm) was adopted. According to [1], the central area of this standardized full-scale specimen (i.e. the seat, the T-transitions on both sides and a part of the cylindrical body on both sides) is fully representative, from the point of view of full-scale test results, of real axles in the regions where the wheels are pre-fitted and the adjacent areas.
To verify the propagation attitude of pre-existing defects under the press-fit, four artificial notches were machined on the press-fit seat. Such notches were manufactured by Electrical Discharge Machining (EDM) at 9 mm from the edge of the press-fit seat (Figure 2b), and spaced with a circumferential extension of 75° and a depth of 350 μm (Figure 2c), which follows the observations reported in [40], being representative of the fretting fatigue damage experimentally observed on real railway axles.

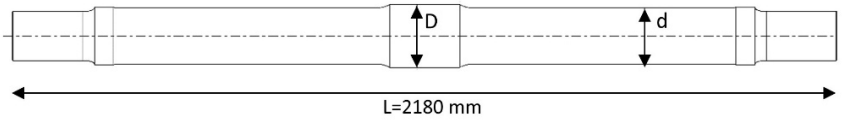

(a)

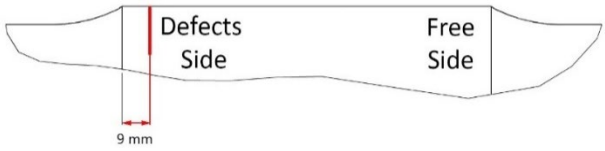

(b)

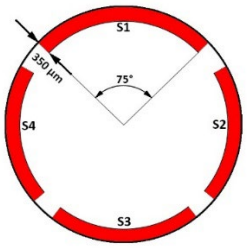

(c)

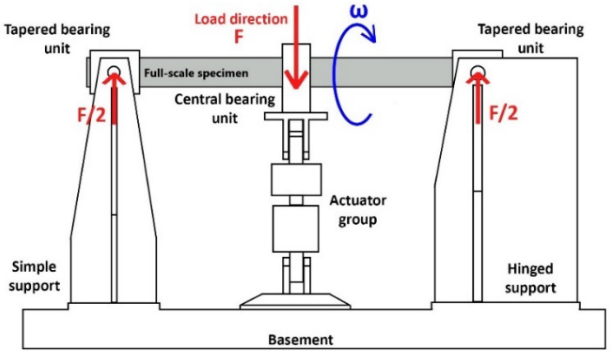

(d)

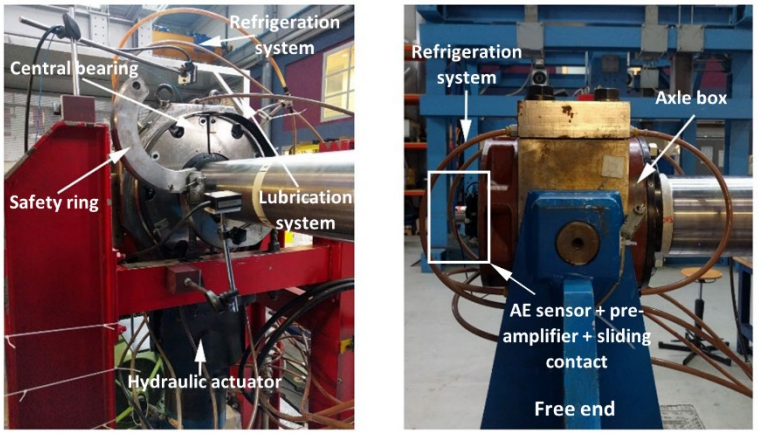

(e)

Figure 2. Experimental setup [13]: (a) full scale specimen; (b) position of artificial notches from the edge of the seat; (c) section of artificial notches on press-fit seat; (d) scheme of the Vitry test bench; (e) Vitry test bench parts.

The test was performed by means of the "Dynamic Test Bench for Railway Axles" (BDA) available at the labs of the Department of Mechanical Engineering at Politecnico di Milano. This bench is a Vitry test rig, i.e. a three-point rotating bending facility (Figure 2d). The ends of the axle are connected to the bench by real axle boxes. One of them is connected to an electric motor applying, to the specimen, a test rotational speed of 509 rpm, which is the typical one of solid axles for freight applications. For the external load application, the central region of the specimen, i.e. the press-fit assembly under test, is connected to a hydraulic actuator (maximum load capacity of 250 kN) by means of a spherical rolling bearing. Since the experimental setup cannot manage and accommodate a real full-scale wheel press-fitted onto the specimen, a special wheel hub (bush), was designed both to introduce the same press-fitting conditions of real applications and to allow the connection to the central spherical rolling bearing of the bench (Figure 2e). It was made of ER7T steel grade, which is one the standardized grades for manufacturing railway wheels in Europe.

The test was divided into two parts characterized by two different nominal stress levels applied to the section of the artificial notches, for a total of 22 x 10^6 applied fatigue cycles. This was done because previous studies showed [41] that, for the considered material and axle geometry, the fretting fatigue strength is approximately 110-120 MPa. At this stress level, a scanning electron microscope (SEM) examination of the contact surface, performed after the conclusion of the tests [41], showed the presence of multiple non-propagating fretting damage sites, suggesting that this stress level represents the incipient fretting fatigue failure. Consequently, to check the performance of AE monitoring in different conditions of damage development, a 108 MPa stress amplitude level was applied for 15x10^6 fatigue cycles to remain close to the fretting fatigue strength, while a 135 MPa stress amplitude level was applied for about 6.5x10^6 fatigue cycles in order to be sure to initiate and propagate fretting fatigue damage.

2.2 Setup for Acoustic Emission monitoring

During the test, the specimen was monitored by AE. It provides two flat surfaces, at its free ends, suitable for coupling an AE sensor, but just one of them could be used (Figure 2e). Therefore, just one piezoelectric sensor was applied (Vallen VS150-M with resonance working frequency in the range 100–450 kHz) using a custom-made mount designed to hold it in position together with a pre-amplifier (Vallen AEP4 34 dB).
The adopted AE sensor was acoustically coupled to the surface of the specimen using OKS-1110 silicone grease and, during the test, such a coupling was periodically secured by the Pencil Lead Break test (PLB) [42]. The PLB test produces a standardized artificial AE burst by breaking a pencil lead (2H hardness, diameter of 0.3 mm and free length equal to 3±0.5 mm) at an angle of 30° on the sample's surface. For this case, the signals originated by PLB test exhibited a clear burst waveform with maximum amplitude of 70 dB.
The rotating measuring group was linked to a sliding contact (Michigan Scientific S4) to send the acquired signals to the AE acquisition system (Vallen AE control unit AMSY-6 with eight channels). The control unit also acquired the number of cycles signal so that each event could be precisely associated to its number of applied fatigue cycles. The management of AE monitoring during the test was performed by Vallen AE-Suite Software R2017.0504.1.
The acquisition chain was also calibrated using the PLB test and the adopted acquisition parameters are reported in Table 1. A discussion is required about the acquisition threshold (Figure 1), which is a critical parameter for AE monitoring because it is the condition triggering the recording of a given signal according to its amplitude value. To set this parameter, along with the acquisition of PLB tests, a characterization of different kinds of background noise was performed. First, the specimen was put in rotation at 509 rpm without load: in this condition, it is expected that the acquired AE signals are just related to noise. Then, electro-magnetic interference was acquired plugging and unplugging the set-up cables. Finally, the interference of the moving bridge crane of the lab was also acquired. All this allowed to set the acquisition threshold to 69 dB, to gather signals like PLB bursts and reduce the acquired amount of useless (noise) data.
During the test, several parametric features of the raw signal were collected for all the recorded (above threshold) AE hits: amplitude, rise time, duration, counts, energy, root mean square, number of applied fatigue cycles, as well as the waveforms.

Table 1. AE acquisition parameters.

Channel	1
Sampling rate for the acquisition of AE features	10 MHz
Sampling rate for the acquisition of AE transient waveforms	5 MHz
Max sample per set	524,288
Pre-Trigger	200 µs
Acquisition threshold (with respect to a reference voltage amplitude of 1 µV)	69 dB
Frequency filter	230-850 kHz
Pre-Amp gain	34 dB
Rearm Time	3.2 µs

3 Non-Destructive Testing

During the test, periodical NDT inspections were performed by PAUT at suitable interruptions for detecting potential damage development and to validate AE monitoring. After the end of the test, the contact surfaces of the specimen were inspected by VT and MT.

3.1 Visual and magnetic particles testing

Figure 3a shows the VT inspection of the circular press-fit area of the specimen unrolled to observe it as a single 2D plane map. The four artificial notches are highlighted, and it was observed:

- lack of evident material removal (wear), typically expected for hard fretting action, and a uniform brightness of the surface. These evidences seem to suggest the damaging action due to the applied test conditions and loads is rather light;
- very small and superficial wear craters are present in the region of notch S1 and are absent anywhere else, including the free side;
- the shiny central region of the seat, where stick conditions between the contact surfaces are expected, is significantly wide;
- dark strips, i.e., black colored regions in correspondence of the transition between stick and slip areas, are present within a narrow region (0-20 mm range) close to the edges of the seat;
- complete lack of scoring, i.e., long scratches in the direction of the press-fit technological process due to an excessive pressure or sliding velocity or to the incorrect choice of the lubricant [43]. Even if this damaging phenomenon is not related to fretting, its lack, usually, suggests a correct press-fitting process.

In conclusion, the press-fit seemed to be technologically well realized and the obtained fretting conditions, during the test, seemed to be not so aggressive and somehow light and limited, at least with respect to other cases shown in the literature [44]-[45].

MT inspections were performed using Elite FW1 fluorescent magnetic particles in liquid suspension (kerosenoil), a transportable electro-magnetic yoke Parker Silver DA-400 and a black light UV lamp. MT confirmed the reported VT conclusions and allowed to detect just two fatigue cracks: a small one located on the free side (Figure 3b), at 3 mm from the edge and having a 4 mm circumferential extension, and a bigger one emanating from both the ends of notch S1 (Figure 3c).
The morphology of the fracture surface of the second crack (Figure 3d, [13]) was observed and analyzed by mechanically opening the specimen after putting it into liquid nitrogen: the clear asymmetric shape suggests that the crack initiated at the right side (in the picture) of the artificial notch and propagated towards the left side. The maximum depth reached at the right side is about 24 mm.

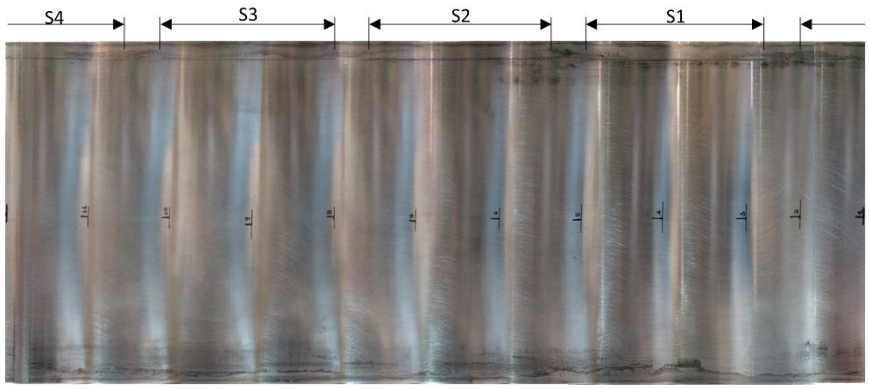
S4
S3
S2
S1

(a)

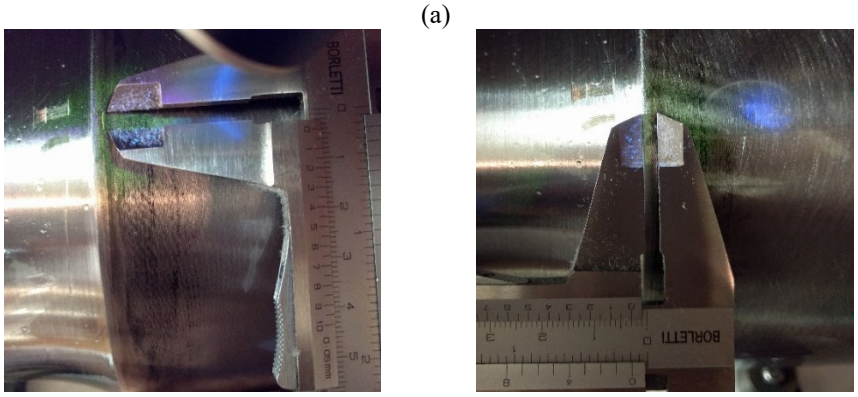
BORLETTI
BORLETTI

(b)

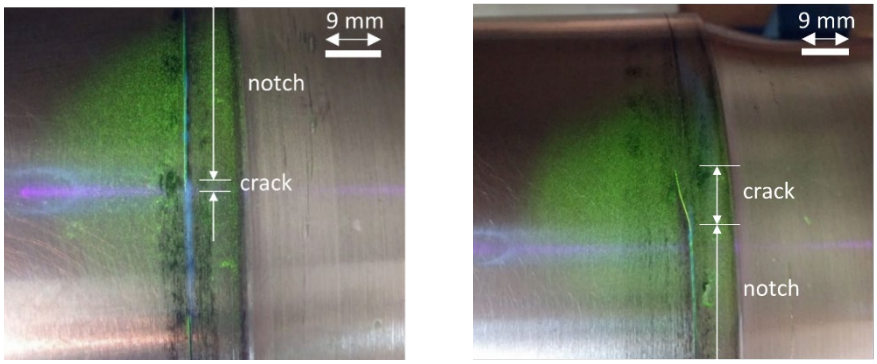
9 mm
notch
crack
9 mm
crack
notch

(c)

(d)

Figure 3: Visual and magnetic particle inspections of the contact surface after the end of the full-scale test: (a) visual inspection (the circular press-fit area of the specimen has been unrolled so that it can be observed, entirely and at the same time, as a single 2D plane map). (b) magnetic particle inspection (small crack at the free side); (c) magnetic particle inspection (crack emanating from notch S1); (d) fracture surface of the crack emanating from notch S1 [13].

3.2 Phased Array Ultrasonic Testing

The application of periodical inspections by PAUT during the test allowed to gather information on the integrity of the specimen to validate the proposed AE monitoring approach.

The adopted equipment consisted of a Harfang X32 phased array unit operating a Harfang T1-PE-5.0M32E0.8P linear probe (nominal frequency 5 MHz, 32 active elements, 0.8 mm pitch) mounted on a concave Rexolite wedge for both matching the flat surface of the probe to the cylindrical external one of the specimen and generating shear ultrasonic waves into the specimen itself. Acoustic coupling was realized by an ultrasonic silicone gel, while the calibration of the time axis showed that the speed of shear waves in the sample was approximately equal to 3520 m/s. PAUT inspections were performed by the reflection (pulse-echo) method and adopting a sectorial scan representation (S-Scan) of the ultrasonic echoes. This because the cylindrical external surface of the specimen is the only available access point (Figure 4) for the PAUT inspection of the press-fit seat without any modification of the testing layout. From this point of view, since both defect and free sides can be affected by damaging phenomena, the following inspection configurations were applied to check the axle at every interruption of the test:

- configuration 1: applied from the free side (“FS”) to inspect the region of artificial notches. The adopted S-Scan ranged from 45° to 70°;
- configuration 2: applied from the defect side (“DS”) to inspect the free side region, adopting the same range.

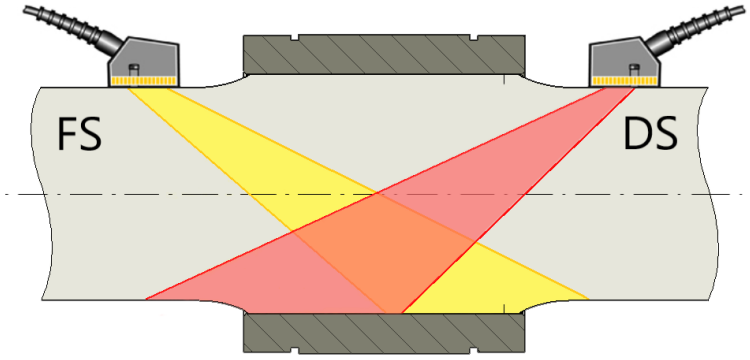

Figure 4. Access points for PAUT inspections of the press-fit seat.

Sensitivity calibration was performed on the echo response of the artificial notches before the beginning of the test and, since the axle is a 3D component and the possible failure locations are not preventively known, all the inspections were exploited on the whole circumferential revolution. Finally, test interruptions, for PAUT inspections, were carried out every 5 x 10^6 fatigue cycles during Part 1 of the test and every 2x10^5 fatigue cycles during Part 2.

First, the interpretation of PAUT S-Scan maps (Figure 5) is explained. To simplify the interpretation of the data, PAUT inspections were performed, on one of the artificial notches, during the disassembling operations, which took place after the end of the test, of the bearing and of the bush from the specimen. Then, technical drawings were superimposed to the maps. Figure 5a shows the PAUT S-Scan map for the case of specimen with bush and central bearing, Figure 5b for the case with just the bush, while Figure 5c for the case of bare specimen. As can be seen, all the echo responses of the geometrical features of the involved components can be easily motivated and recognizable, while the remaining ones are associated to internal reflections of the ultrasonic beam. It is also remarkable the disappearance of echo responses with the progressive removal of components, until reaching the bare condition, which shows just the echo response due to the artificial notch.

PAUT inspections detected the crack emanating from notch S1 (see Figure 5b) at about 19 x 10^6 applied fatigue cycles. The estimation of crack depth was carried out by the “crack tip diffraction” method [46] and resulted to be approximately 1 mm. Then, such a crack went on propagating and increasing its size till the end of the test: Figure 5d and Figure 5e show the comparison of response echoes at 0 applied fatigue cycles and at 21.5 x 10^6 applied fatigue cycles. The final estimation of crack depth resulted to be approximately 20 mm at the deepest point, slightly undersized with respect to fractography (see Figure 3d).

On the other hand, PAUT inspections were not able to detect the small crack found by MT on the free side of the seat. This just means the size of that crack was still below the sensitivity level of the adopted PAUT inspection procedure.

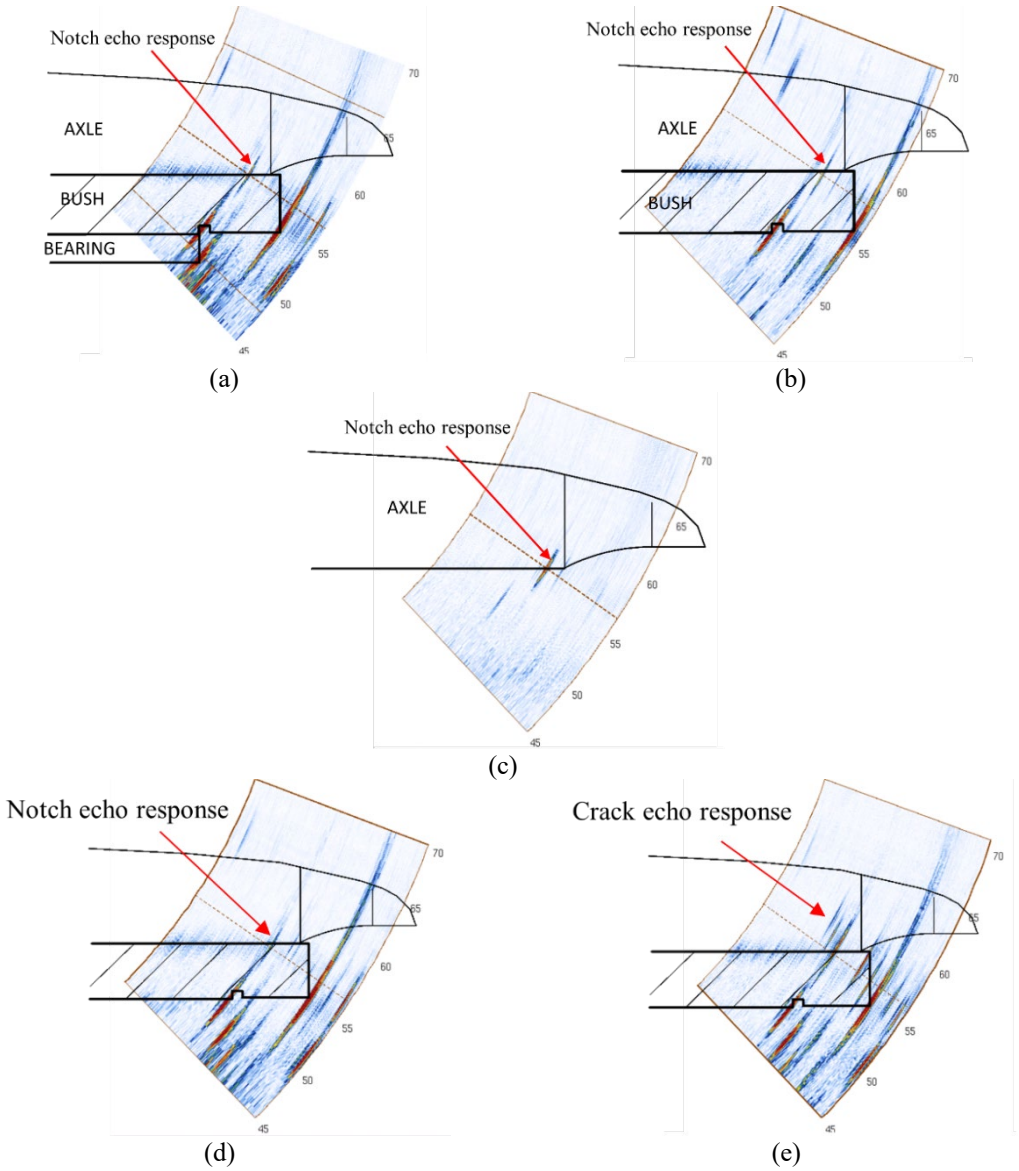

Figure 5. Interpretation of S-Scan maps: (a) case of axle with bush and central bearing; (b) case of axle with bush; (c) case of bare axle: (d) notch S1 (configuration 1) at 0 applied fatigue cycles; (e) notch S1 (configuration 1) at 21.5 x 10^6 applied fatigue cycles.

4 Post-processing of Acoustic Emission raw data

Figure 6 shows the collected AE raw data, in terms of amplitude vs. number of fatigue cycles and where each green dot represents a recorded AE hit (in total, about 670,000), as well as the time history of the applied stress. No hits having amplitude lower than 69 dB were collected, because of the chosen acquisition

threshold. The variation of the applied stress, switching from Part 1 to Part 2 of the test, was not very evident observing the AE activity: an expected peak of events is clearly seen at the exact number of fatigue cycles of the applied stress variation, but then, not so much more activity followed during Part 2 of the test.

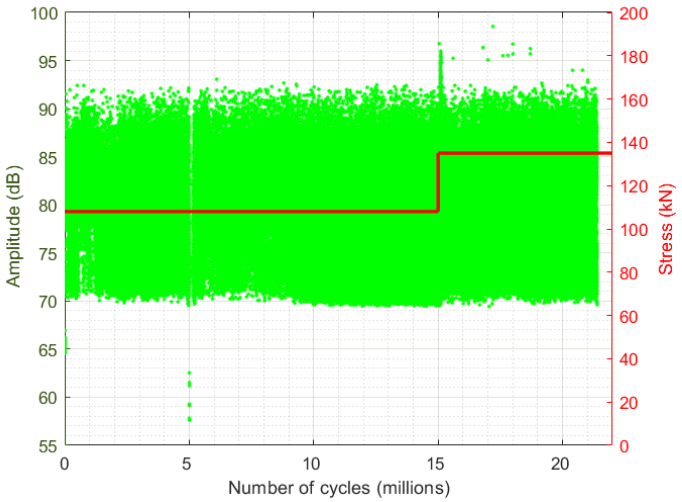

Figure 6. AE raw data collected during the whole full-scale test, in terms of amplitude vs. number of fatigue cycles, and the time history of the applied stress.

To cluster the recorded AE hits according to fretting damage or background noise, a pattern recognition technique, named "automatic k-SOM", was adopted. This algorithm, described in [47] and fully validated in [48], was chosen because it was previously successfully applied to AE monitoring of rotating bending fatigue cracks in railway axles [29]. It is based on an unsupervised clustering approach implementing a specific ANN named Self-Organizing Map (SOM) [49]. SOM is a bivariate topological map having a hexagonal lattice with a sheet structure and a Gaussian neighborhood function: based on a set of selected features relevant for the considered case, similar samples are mapped close together and dissimilar ones are mapped far apart. This may be visualized by a U-Matrix (Unified Distance Matrix), which represents the Euclidean distance between weight vectors of neighboring cells. The observation of the U-Matrix allows to appreciate the degree of separation among groups (clusters) of similar signals. It is, then, possible to extract and build such clusters applying simple clustering algorithms, such as the k-means one [50], to the U-Matrix. However, the big issue consists in choosing, a priori, the optimal number of clusters. Indeed, once the SOM is trained and the U-Matrix drawn, deciding the optimal number of clusters for the input dataset stands to the user. It is to solve this issue that the automatic k-SOM clustering algorithm was used in [29] and is adopted in this work. This algorithm is an evolution of the traditional SOM approach and evaluates automatically the best performing number of clusters a priori, based on the combination of a few quality indexes for clustering processes. More in detail, after training the SOM, the U-Matrix is clustered by the k-means algorithm considering a number of clusters "c" ranging from 2 to 15. For each c case, the quality of clustering is, then, evaluated computing an aggregate index L_i based on three different performance indexes: the Davies-Bouldin [51], the Silhouette [52] and the Calinski-Harabasz [53]. This allows to mitigate the cons and to strengthen the pros of each single index. The optimal number of clusters

is the one showing the higher value of the aggregated index L_i. Finally, the k-means algorithm is applied to the U-Matrix to cluster the data into the estimated optimal number of clusters.
For the application of the k-SOM algorithm to the present AE raw data, all the time domain features, shown in Figure 1, and some frequency domain features (frequency peak amplitude, frequency centroid) of the recorded AE waveforms were inputted to the algorithm. The optimal number of clusters was estimated (Figure 7) to be equal to 2 and the clustering process defined Cluster 1 containing 104,338 AE hits (15.6% of the total), and Cluster 2 containing the remaining 565,858 ones (84.4% of the total). It seems reasonable to assume that one cluster is related to fretting fatigue damage, while the other one to background noise.

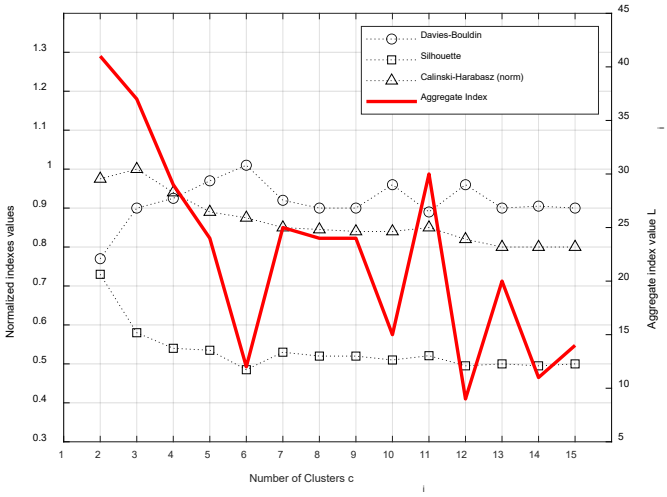

Figure 7. Estimation of the optimal number of clusters for AE raw data.

To define the physical meaning of the identified clusters of AE hits, the charts of cumulated energy (Figure 8a) and of cumulated AE activity (i.e., the number of AE hits, Figure 8b) over time, i.e., over the progressive application of fatigue cycles, are first analyzed. For data clustered into Cluster 1, Figure 8 highlights a nearly constant and time-independent increasing trend involving a small number of low-energy signals: these features well represent the expected behavior of background noise. On the other hand, for AE hits clustered into Cluster 2, the same figure highlights the presence of time-dependent and steep events, especially a main one occurring between $12x10^6$ and $13x10^6$ cycles, characterized by a significantly high increment of energy and activity: these rather instantaneous events well represent the expected behavior of a developing damage, i.e. a nearly instantaneous release of a large amount of elastic energy due to phenomena such as plasticization, fracturing, … It is known from the literature [54], and it was fully confirmed in the case of crack propagation at the free external body surface of solid axles [29], that crack initiation and final fracture are typically characterized by a high and sudden AE activity with signals having a high energy level, while the propagation stage is usually rather silent. Since the final fracture stage was not reached during the test, the sudden increments of cumulated energy and AE activity, shown in Figure 8, seem to suggest the occurrence of crack initiation(s). Nevertheless, the regions of the cumulated energy and activity curves of Cluster 2, before and after the main AE event occurring between $12x10^6$ and $13x10^6$ cycles, are generally characterized by a mild slope similar (parallel) to each other and similar (parallel) to the trend of the data clustered in Cluster 1: this seems to suggest that, before the main AE event, just the

first stage of a fretting wear action was emitting AE hits, while, after the main AE event, crack propagation was taking place. It remains that the AE events occurring before and after the main AE event, even if very similar in terms of cumulated energy and activity, were divided into two distinct clusters, suggesting relevant differences lie in other features characterizing the waveforms.

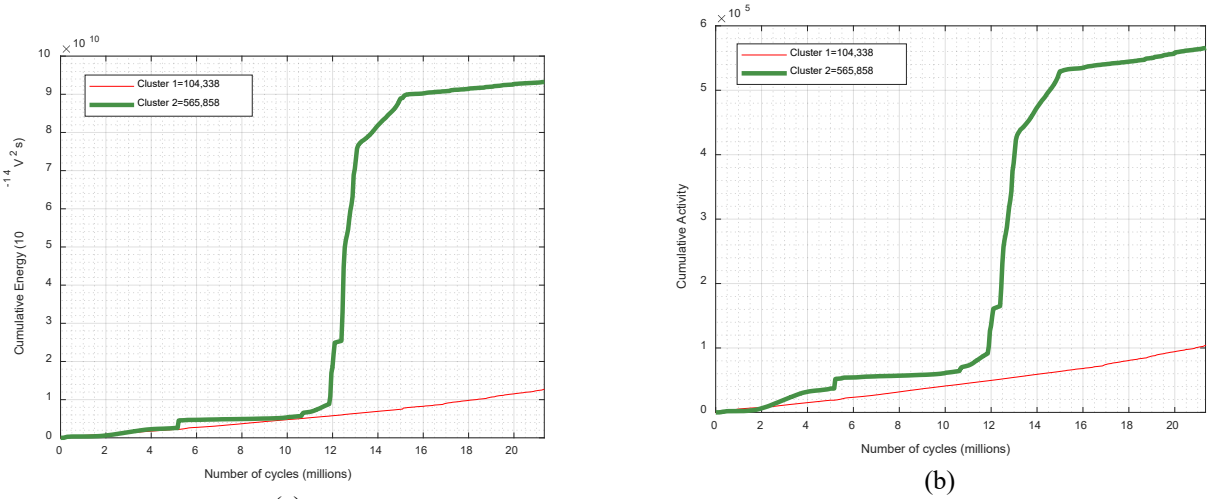

(a) (b)

Figure 8. Automatic k-SOM results in terms of cumulated features of clustered data: (a) energy; (b) AE activity (number of hits).

To support further the interpretation of the defined clusters, the waveforms were analyzed. Figure 9 shows the comparison of some examples of both clusters extracted at the beginning ($5.2x10^6$ cycles), during the main AE event ($12.5x10^6$ cycles) and at the end ($20.3x10^6$ cycles) of the test. As can be seen, a relevant morphological difference of the waveforms belonging to the two clusters is evident at any stage of the test. Waveforms in Cluster 1 (Figure 9a, Figure 9c and Figure 9e) show the typical morphology of a "continuous emission" having a low amplitude level and a relatively short time duration: these features confirm the results drawn from the analysis of the cumulated charts reported above, because they are commonly ascribed to background noise [33]-[34], which, during a test is expected to be constant and continuous with time. Also, no relevant differences between the waveforms in Cluster 1 can be observed considering the beginning, during the main AE event or the end of the test and this is another proof of the independence of the signals included in this cluster with respect to the occurrence of possible sudden damage phenomena such as crack initiation. On the other hand, waveforms in Cluster 2 (Figure 9b, Figure 9d and Figure 9f) show the typical morphology of a "burst emission" with transient behavior and, with respect to the signals included in Cluster 1, a higher amplitude level and number of counts and a significantly longer time duration. Moreover, some features of the clustered waveforms, e.g. the amplitude, change considerably during the test, especially comparing the main AE event to the initial and final parts. These considerations confirm the interpretation of the clusters and explain why similar waveforms, in terms of cumulated energy and activity, were clustered differently.

To sum up, the time independent Cluster 1, with low constant amplitude waveforms and regularly increasing cumulated energy and activity, is identified as background noise, whereas the time dependent Cluster 2, with transient high amplitude waveforms and an irregular trend for the cumulated energy and activity, is identified as fretting fatigue damage.

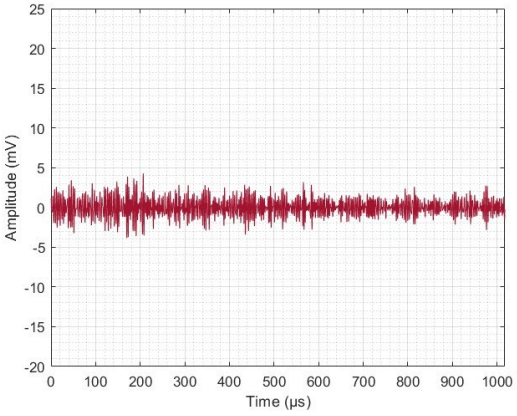

(a) – Cluster 1 – 5.2x10^6 fatigue cycles

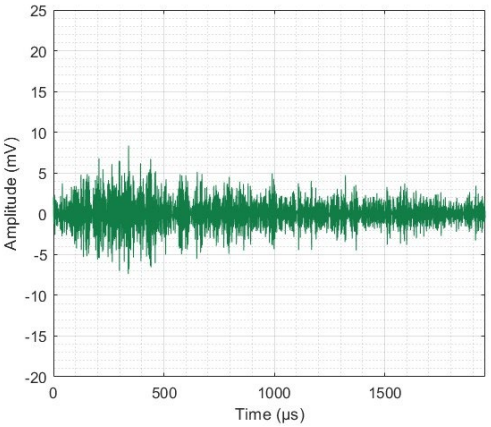

(b) – Cluster 2 – 5.2x10^6 fatigue cycles

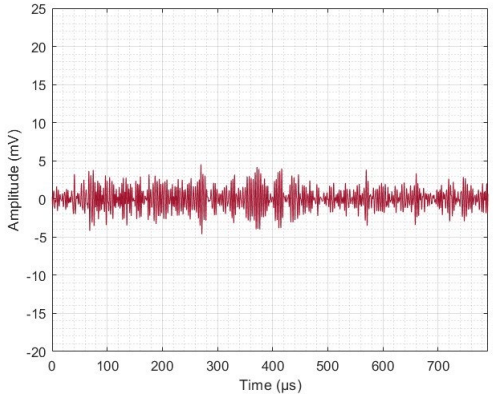

(c) – Cluster 1 – 12.5x10^6 fatigue cycles

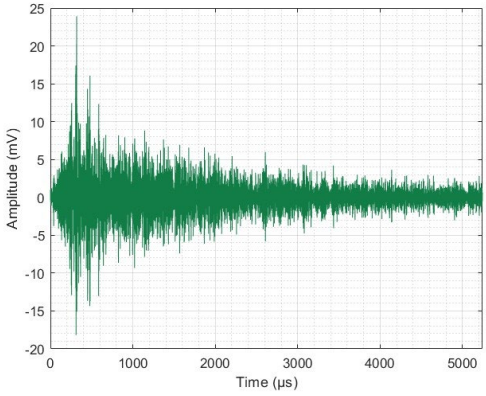

(d) – Cluster 2 – 12.5x10^6 fatigue cycles

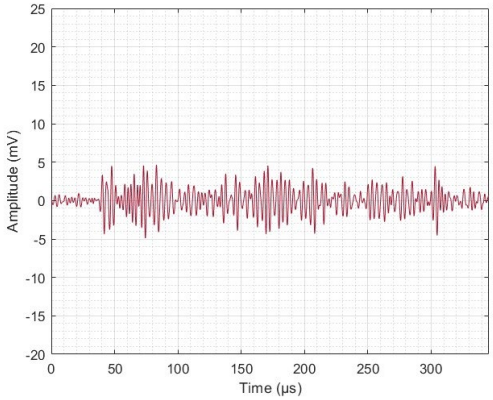

(e) – Cluster 1 – 20.3x10^6 fatigue cycles

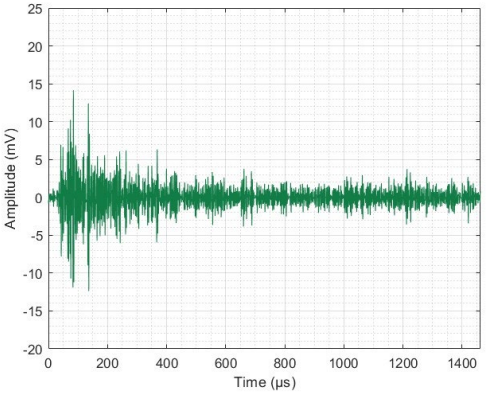

(f) – Cluster 2 – 20.3x10^6 fatigue cycles

Figure 9. Examples of waveforms recorded during the full-scale test.

5 Discussion

For all the above, just Cluster 2 is considered for the discussion on AE monitoring during the test. Observing charts in Figure 8, a very limited number of sudden increments of energy and activity, and consequently of expected crack initiations, occurred during the test. As seen in Section 3.1, this interpretation was subsequently confirmed and validated by the inspections performed by MT, which just detected a small crack on the free side of the press-fit seat and a bigger one emanating from both the ends of notch S1. Even if qualitative, this is a first important validation.
It seems reasonable to ascribe the main AE event occurring between $12x10^6$ and $13x10^6$ cycles (Figure 8) to the initiation of the big crack emanating from both the ends of notch S1, because it is the only "big thing" which actually happened during the test. It is very difficult, instead, to separate and identify the AE activity directly related to the initiation of the small crack located on the free side of the press-fit seat. Unfortunately, this is one of the limitations of AE monitoring: all the occurring AE events are mixed up in the acquisitions and it is rather difficult to identify each single occurrence of crack initiations, especially if they are numerous and at the very beginning, i.e. when their contribution to the increment of cumulated energy and activity is still rather small, as in the case of the present small crack located on the free side of the press-fit seat. It is likely this issue might be mitigated and partially solved exploiting the possibility to localize the sources of each AE event by triangulating signals arriving to multiple sensors, but this remains an open point of this research. It is also observed that the propagation stage is rather silent and, consequently, not much informative. Anyway, it remains that sudden increments of AE energy and activity are easily detectable during AE monitoring and the possibility to relate and ascribe them to crack initiations proved to be effective and promising for evaluating the structural integrity of solid axles subject to fretting fatigue. It can be concluded that the successful detection, during in-service monitoring, of such sudden increments of AE energy and activity would allow triggering safety alarms or warnings and the mandatory application of deeper investigations.
Finally, comparing AE monitoring to PAUT inspections, PAUT could detect the crack after about $19x10^6$ applied cycles, i.e. when the crack had been subjected to enough fatigue cycles to initiate and propagate up to a size exceeding the sensitivity level set by the adopted PAUT inspection procedure. AE monitoring detected a relevant damage between $12x10^6$ and $13x10^6$ cycles, which is much earlier than PAUT. This is due to the inherent and unique property of AE monitoring to be sensitive to crack initiation and not to crack size, as PAUT and all the other NDT techniques do. This is an undeniable advantage with respect to the state of the art on the inspection and monitoring of railway axles in general and subject to fretting fatigue damage in particular. Even if some issues are still to be solved, the obtained results are definitely promising and encouraging.

6 Conclusions

In this work, the SHM, by AE, of fretting fatigue damage in a solid railway axle is investigated. To the aim, a full-scale fretting fatigue test was performed and a procedure, based on an unsupervised intelligent classification system using ANN, was applied to post-process AE raw data. This allowed to effectively cluster the acquired signals as either fretting damage or background noise and to highlight sudden increments of cumulated energy and of cumulated AE activity related to crack initiation due to fretting fatigue damage.
The results of the study were validated by other NDT techniques (PAUT and MT testing) and allowed also to understand that the proposed AE approach can detect fretting fatigue crack initiation much earlier than the traditional inspection methods.

Declaration of conflicting interests

The authors declare that they have no known competing financial interests or personal relationships that could have appeared to influence the work reported in this paper.

Acknowledgements

The authors would like to thank Prof. S. Beretta (Dept. Mechanical Engineering – Politecnico di Milano, Italy) and Mr. S. Cantini (Lucchini RS SpA, Italy) for the given support and the useful discussion and Mr. S. Bertozzi for the active help given to the research.

PoliNDT (Interdepartmental Lab for Non-Destructive Testing and Structural Health Monitoring set at Politecnico di Milano) is also acknowledged for providing the acoustic emission equipment.

M. Zamorano thanks Universidad Carlos III de Madrid for funding the visiting period at Politecnico di Milano to collaborate on the research work.

ORCID ID

M. Carboni: 0000-0003-0828-9067

M. Zamorano: 0000-0003-1478-5673

References

1. EN 13261:2020. Railway applications – Wheelsets and bogies – Axles – Product requirements. CEN.
2. EN 13260:2020. Railway applications – Wheelsets and bogies – Wheelsets – Product requirements. CEN.
3. EN 13103-1:2017. Railway applications – Wheelsets and bogies – Part 1: Design method for axles with external journals. CEN.
4. EN 13103-2:2020. Railway applications – Wheelsets and bogies – Part 2: Design method for axles with internal journals. CEN.
5. AAR. Manual of standards and recommended practices, Section G: wheels and axles, AAR, 2020.
6. Waterhouse RB. *Fretting corrosion*. Oxford: Pergamon Press Ltd, 1972.
7. Waterhouse R. Fretting fatigue. *Int Mater Rev* 1992; 37(1): 77–98.
8. Szolwinski MP and Farris TN. Mechanics of fretting fatigue crack formation. *Wear* 1996; 198(1–2): 93–107.
9. Gao JW, Dai X, Zhu SP, et al. Failure causes and hardening techniques of railway axles – A review from the perspective of structural integrity. *Eng Fail Anal* 2022; 141: 106656.
10. Nesládek M, Španiel M, Jurenka J, et al. Fretting fatigue – experimental and numerical approaches. *Int J Fatigue* 2012; 44: 61–73.
11. Ekberg A. Fretting fatigue of railway axles – Review of predictive methods and an outline of a finite element model. *Proc Inst Mech Eng F* 2004; 218(4): 299–316.
12. Foletti S, Beretta S and Gürer G. Defect acceptability under full-scale fretting fatigue tests for railway axles. *Int J Fatigue* 2016; 86: 34–43.

13. Foletti S, Beretta S, Bertozzi F, et al. Experiments on crack propagation and threshold at defects in press-fits of railway axles. *Procedia Structural Integrity* 2017; 7: 484-491.
14. Gürer G and Gür CH. Failure analysis of fretting fatigue initiation and growth on railway axle press-fits. *Eng Fail Anal* 2018; 84: 151–166.
15. Zeng D, Zhang Y, Lu L, et al. Fretting wear and fatigue in press-fitted railway axle: A simulation study of the influence of stress relief groove. *Int J Fatigue* 2019; 118: 225–236.
16. Pourheidar A, Regazzi D, Cervello S, et al. Fretting fatigue analysis of full-scale railway axles in presence of artificial micro-notches. *Tribol Int* 2020; 150: 106383.
17. Zou L, Zeng D, Zhang Y, et al. A coupled wear and crack initiation-propagation methodology for fretting fatigue life assessment in press-fitted axles. *Int J Fatigue* 2022; 159: 106817.
18. Zou L, Lu L, Li Y, et al. Experimental and numerical study on press-fitted railway axles: Fretting fatigue behaviour in the very high cycle regime. *Int J Fatigue* 2023; 166: 107243.
19. Cantini S and Beretta S. *Structural reliability assessment of railway axles*. Series LRS Techno Volume 4, 2011.
20. Cantini S. *Transforming maintenance with data*. Series LRS Techno Volume 14, 2022.
21. Grandt Jr. AF. *Fundamentals of structural integrity*. John Wiley & Sons, 2004.
22. EN 15313:2016. Railway applications – In-service wheelset operation requirements – Inservice and off-vehicle wheelset maintenance. CEN.
23. Chang FK. Structural Health monitoring: A summary report. In: *Proc. 2nd international workshop on structural health monitoring*, Stanford, US, 1999.
24. Boller C. Ways and options for aircraft structural health management. *Smart Mater Struct* 2001; 10: 432–440.
25. Jiang CH, You W, Wang LS, et al. Real-time monitoring of axle fracture of railway vehicles by translation invariant wavelet. In: *Proc. International conference on machine learning and cybernetics*, Guangzhou, China, 2005.
26. Deng XJ, Xui GJ and Liu SQ. Research on fatigue crack detection of rail vehicle axle based on acoustic emission. In: *Proc. 10th international workshop on structural health monitoring*, Stanford, US, 2015.
27. Jiang CH, Pan S, Zhang C, et al. Experimental research on fault location for the axle of railway vehicles based on acoustic emission technique. *Int J Cont Autom* 2016; 9: 91–98.
28. Zhou Y, Lin L, Wang D, et al. A new method to classify railway vehicle axle fatigue crack AE signal. *Appl Acoust* 2018; 131: 174–185.
29. Carboni M and Crivelli D. An acoustic emission based structural health monitoring approach to damage development in solid railway axles. *Int J Fatigue* 2020; 139: 105753.
30. Rolek P, Bruni S and Carboni M. Condition monitoring of railway axles based on low frequency vibrations. *Int J Fatigue* 2016; 86: 88–97.
31. Gómez MJ, Castejón C and García-Prada JC. New stopping criteria for crack detection during fatigue tests of railway axles. *Eng Fail Anal* 2015; 56: 530–537.
32. Chong SY, Lee JR and Shin HJ. A review of health and operation monitoring technologies for trains. *Smart Struct Syst* 2010; 6: 1079–1105.
33. Ohtsu M. *Theory and Characteristics of Acoustic Emission*. Morikita Pub., 1998.
34. Grosse C and Ohtsu M. *Acoustic emission testing*. Springer-Verlag, 2008.
35. Deshpande A and Kumar M. *Artificial Intelligence for Big Data*. Packt Publishing, 2018.
36. Ramirez-Jimenez CR. Identification of failure modes in glass/polypropylene composites by means of the primary frequency content of the acoustic emission event. *Comp Science Tech* 2004; 64: 1819–1827.
37. Anastasopoulos AA and Philippidis TP. Clustering Methodologies for the evaluation of AE from Composites. *J Acoust Emiss* 1995;13: 11-22
38. Schmerr LW. *Fundamentals of Ultrasonic Phased Arrays*. Springer-Verlag, 2015.

39. Caudill M. Neural Networks primer, part I. *Al Expert* 1987; 2(12): 46-52.
40. Hirakawa K, Toyama K and Kubota M. The analysis and prevention of failure in railway axles. *Int J Fatigue* 1998; 20(2): 135–144.
41. Cervello S. Fatigue properties of railway axles: New results of full-scale specimens from Euraxles project. *Int J Fatigue* 2016; 86: 2–12.
42. ASTM E976:2015. Standard guide for determining the reproducibility of acoustic emission sensor response. ASTM International.
43. Benuzzi D and Donzella G. Prediction of the press-fit curve in the assembly of a railway axle and wheel. *Proc Inst Mech Eng F* 2004; 218: 51–65.
44. Guzowski S and Michnej M. Fretting wear in the wheel–axle joint of a wheel set with an automatic gauge change system. In: *Czasopismo Techniczne* 2015; Y. 112,3-M: 3-52.
45. Wulpi DJ. *Understanding how components fail*. ASM international, 2013.
46. Krautkrämer J and Krautkrämer H. *Ultrasonic testing of materials*. 4th ed. Springer-Verlag, 1990.
47. Crivelli D, Guagliano M and Monici A. Development of an artificial neural network processing technique for the analysis of damage evolution in pultruded composites with acoustic emission. *Compos B* 2014; 56: 948–59.
48. Crivelli D. *Structural health monitoring with acoustic emission and neural networks*. PhD Thesis, Politecnico di Milano, Italy, 2014. Open access at https://www.politesi.polimi.it/handle/10589/89521.
49. Kohonen T. The self-organizing map. *Proc IEEE* 1990; 78(9): 1464–1480.
50. Haykin S. *Neural networks and learning machines*. Pearson International Edition, 2009.
51. Davies DL and Bouldin DW. A cluster separation measure. *IEEE Trans Pattern Anal Mach Intell* 1979; 2: 224-227.
52. Rousseeuw PJ. Silhouettes: a graphical aid to the interpretation and validation of cluster analysis. *J Comput Appl Math* 1987; 20: 53-65.
53. Calinski T and Harabasz J. A dendrite method for cluster analysis. *Commun Stat Theory Methods* 1974; 3(1): 1-27.
54. Marfo A, Chen Z and Li J. Acoustic emission analysis of fatigue crack growth in steel structures, *J Civ Eng Constr Technol* 2013; 4(7): 239–249.